

Article

Investigation of Microstructure and Photocatalytic Performance of a Modified Zeolite Supported Nanocrystal TiO₂ Composite

Gang Liao ^{*,†}, Wei He [†] and Yuming He

Department of Transportation and Municipal Engineering, Sichuan College of Architectural Technology, Chengdu 610399, China; scacfloyd@126.com (W.H.); scachym@163.com (Y.H.)

* Correspondence: liaogang@scac.edu.cn; Tel.: +86-28-69514351

† These authors contributed equally to this work.

Received: 9 May 2019; Accepted: 30 May 2019; Published: 31 May 2019



Abstract: A modified zeolite/TiO₂ composite (MZTC) was prepared through a method of saturated infiltration and synthesis in situ. The crystalline phase, micromorphology, elementary composition, specific surface area, pore size distribution, chemical bond and band gap variation of the products were characterized by X-ray diffraction (XRD), scanning electron microscopy (SEM), energy dispersive spectroscopy (EDS), BET specific surface area and pore size distribution analysis (BET), Fourier transform infrared spectroscopy (FTIR) and UV–vis diffuse reflectance spectroscopy (UV-vis DRS), respectively. The microscopic characterization results showed that TiO₂ was homogeneously dispersed in the structure of zeolite at the nanoscale range, and a strong chemical bond was established between TiO₂ and zeolite. The photocatalytic performance of MZTC was evaluated by studying the degradation rate of methylene blue (MB) dye in aqueous solution under UV-light irradiation. The results of the degradation experiment showed that the MB degradation rate of MZTC-2.5 was the highest, reaching 93.6%, which was 2.4 times higher than hydrolysis TiO₂ powder (HTOP) containing the same mass of pure TiO₂. The MB degradation rate of MZTC-2.5 still maintained 86.5% after five tests, suggesting the excellent recyclability of MZTC-2.5. The possible mechanism of MB degradation was also discussed.

Keywords: modified zeolite/TiO₂ composite; saturated infiltration; synthesis in situ; photocatalytic performance

1. Introduction

In recent decades, the water pollution caused by organic contaminants, such as dyes, antibiotics, polycyclic aromatic hydrocarbons and phenols, is becoming a serious concern worldwide [1–4]. Scientists have carried out numerous solutions to control the water pollution and several achievements have been made [5–10]. Nowadays, whatever technique is applied to purify the contaminated water, consideration must be given to purification efficiency, cost, operability, and durability. Photocatalytic oxidation (PCO) based on TiO₂ displays excellent prospects in environmental purification owing to its high efficiency, non-toxicity, low cost, and chemical stability [11–14]. It is well known that reactive oxygen species (ROS) like ·OH radicals generated on the surface of TiO₂ bear strong oxidative power, so most organic-based compounds undergo complete mineralization to end products such as H₂O and CO₂. To enhance the photocatalytic activity, TiO₂ is usually fabricated into nanoparticles or a one-dimensional (1-D) fibrous structure and modified by doping heteroatoms or introducing noble metals [15–17]. Although the photocatalytic performance has been improved, there are new challenges appearing along with the wide application of nano-TiO₂. The TiO₂ nanoparticles are easily agglomerated in water due to high surface energy, which leads to a reduction in photocatalytic

efficiency [11]. There is evidence that TiO₂ nanoparticles are discharged into aquatic ecosystems during their application [18]. If the nanoparticle can not be removed from water, TiO₂ will enter drinking water sources and natural aquatic environments, increasing the risk of exposure to plants, animals and humans [19]. The adsorption capacity of the catalyst towards the pollutant governs the photocatalytic decomposition efficiency, especially at low concentrations. The photocatalytic efficiency of TiO₂ is often limited due to its low adsorption ability as well as the low concentration of pollutants in ambient water [20–22]. To deal with these new challenges, it is vital to firmly immobilize TiO₂ nanoparticles on the substrate and improve the adsorption of the catalyst.

Many materials have been utilized for supporting TiO₂ [21,23–26], among which natural zeolite (NZ) was proven to be the most desirable supporting material due to its high specific surface area, high adsorption capacity, and high stability [27–29]. Zeolite supported nano-TiO₂ composites have been intensively studied for years and research shows that the hybrid zeolite/TiO₂ composites exhibit good photocatalytic degradation performance [24,30–33]. According to previous works, the outstanding adsorptive ability of zeolite has been commonly used to enhance the photocatalytic activity of zeolite/TiO₂ composites, because zeolites act as electron donors and acceptors of moderate strength to the guest species based on the adsorption site and could enrich the pollutants around TiO₂ and then accelerate the photocatalytic rate [34–36]. The level and nature of the interaction of zeolite and TiO₂ determine the microstructures of the zeolite/TiO₂ composite, which deeply influence the photocatalytic performance. Domoroshchina et al. [20] thought the interaction between components depends on the methods and conditions for obtaining nanocomposites. There are numerous cavities in the framework of zeolite which can not only act as adsorbers, but provide the possibility to enhance the interaction of TiO₂ and zeolite. Currently, most zeolite/TiO₂ composites have been synthesized through the sol-gel method at normal pressure and temperature, which is easy to realize [37–40]. However, most zeolite/TiO₂ composites are a mixture of TiO₂ and zeolite with altered microstructural characteristics, which is not enough to exploit the advantages of zeolite/TiO₂.

In the present study, the aim is to synthesize a composite with high efficiency and stable properties. The method of saturated infiltration and synthesis in situ was proposed. Different from the conventional sol-gel method, NZ was firstly immersed in the TiO₂ sol under negative pressure to ensure every cavity was filled with sol and then nanocrystal TiO₂ was formed in situ under heat treatment. The physical and chemical properties of MZTC were investigated using a variety of micro characterization methods. The photocatalytic efficiency of MZTC was evaluated by degrading methylene blue (MB) in aqueous solution, which is a representative organic pollutant in the textile wastewater industry.

2. Results and Discussion

2.1. Physicochemical Properties

X-ray diffraction (XRD) patterns of the samples are shown in Figure 1. Compared with commercial TiO₂ (P25), HTOP prepared by the sol-gel route is proved to be anatase TiO₂. The crystallite size of the HTOP and P25 are about 10 nm and 25 nm, respectively, as calculated by the Scherrer equation [17]. The phase compositions of NZ, MZ and MZTC-2.5 are SiO₂ and K_{2.04}Na_{0.06}Al₂Si_{7.8}O_{20.7}. The intensity of the diffraction peaks of MZ and MZTC-2.5 are weaker than NZ, because the Si in the zeolite skeleton was selectively dissolved and the chemical-bonding water was destroyed. The X-ray pattern of MZTC-2.5 is almost the same as MN and the characteristic peaks of TiO₂ are not observed in the diffraction patterns of MZTC-2.5, which may contribute to the low content and small size of TiO₂. The absence of TiO₂ characteristic peaks indicate that the nanocrystal TiO₂ are well dispersed on the zeolite surface and the growth of large-size TiO₂ crystallites is prevented [41], which is conducive to improve the photocatalytic activity of MZTC [42].

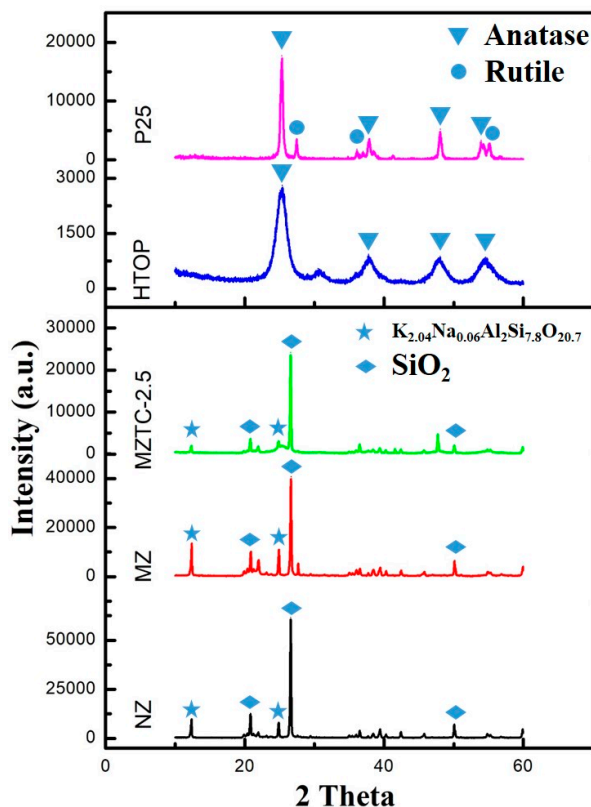


Figure 1. X-ray diffraction patterns. (a.u. = arbitrary units).

Figure 2a,b show the scanning electron microscopy (SEM) images of P25 and HTOP, respectively. It can be observed that P25 is stacked with nanoparticles with a diameter of approximately 25 nm, which is in accordance with the XRD result. The HTOP is of block shape and the TiO₂ particles are compacted after calcination of 400 °C. Figure 2c,d show the morphologies of NZ and MZ, respectively. It can be clearly seen that NZ is formed from stacking plate-like units and the surface is regular and smooth. After modification, the surface of MZ is irregular and rough and many micron-sized cavities can be observed. This is because the impurities in the pore were removed, leading to an open and clear pore system, which contribute to the diffusion and adsorption of the pollutant. Figure 2e shows the morphologies of MZTC-2.5. It can be seen that the microstructures of MZTC-2.5 were almost same as MZ and the agglomeration of TiO₂ was not observed on the surface of MZTC-2.5, which was also identified by the XRD results. Combined with the micrograph of HTOP, it can be inferred that the absence of the agglomeration of TiO₂ was due to the interaction of TiO₂ and zeolite, which inhibits the growth of large-size TiO₂ crystallites and the agglomeration of TiO₂ particles. Three random points on the surface of MZTC-2.5 were selected for energy dispersive spectroscopy (EDS) analysis, the results of which are shown in Figure 2f–h. The content of Ti at each point exceeded 10%, which confirmed that the nano-TiO₂ had already been deposited on the structure of MZTC-2.5. The Ti content of the three points was approximately equal to each other, indicating the uniform distribution of TiO₂.

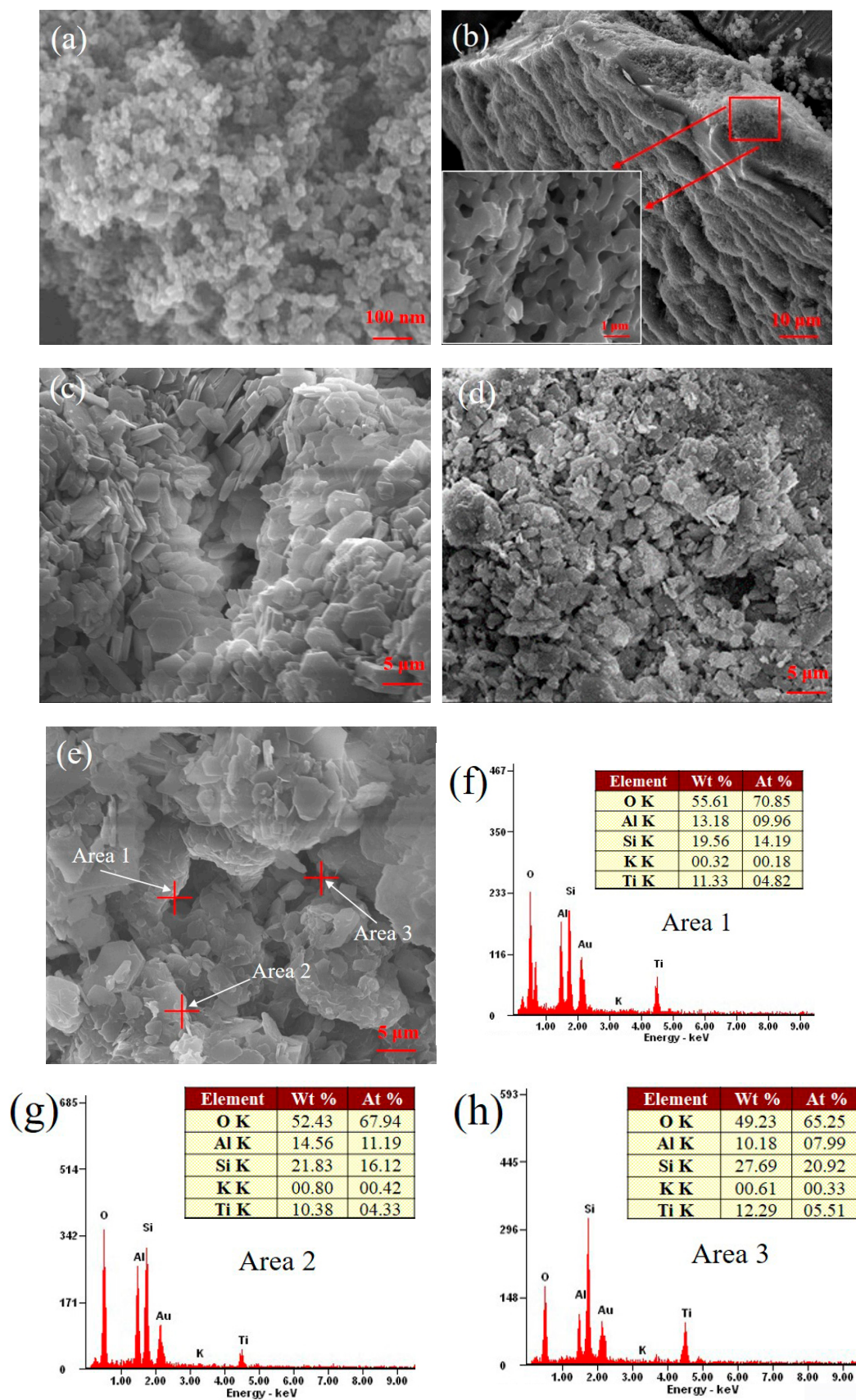


Figure 2. Scanning electron microscopy (SEM) images: (a) P25; (b) HTOP; (c) NZ; (d) MZ; (e) MZTC-2.5; energy dispersive spectroscopy (EDS) results of MZTC-2.5: (f–h).

The nitrogen adsorption–desorption isotherms of MZ and MZTC-2.5 are presented in Figure 3a. For MZ, the isotherm is of type III and IV (BDDT classification) [43,44]. At low relative pressure, the adsorbed volume of N₂ is small, indicating the absence of micropores or the weak force between MZ and N₂ (type III). However, at a high relative pressure range (between 0.3 and 0.9), the isotherm displays a small hysteresis loop, confirming the presence of mesopores (type IV). This is also demonstrated by its corresponding pore-size distribution curve in Figure 3b. The shape of the hysteresis loop is of type H3, which is associated with the stack of plate-like particles, generating slit-like pores [44]. This is also confirmed by the SEM images of MZ. Loading nano-TiO₂ on the surface of MZ causes a certain influence on the isotherm. The shape of the isotherm of MZTC-2.5 is similar to MZ, but the hysteresis loop of MZTC-2.5 is larger, suggesting that the pore size distribution range of MZTC-2.5 is wider. This is in accordance with the pore-size distribution curves in Figure 3b. Moreover, the specific surface area of MZTC-2.5 (293 m²g⁻¹) is lower than that of MZ (392 m²g⁻¹), as shown in Table 1. This is closely related to the changes of the pore system of MZ. After saturated infiltration and calcination, the mesopores in MZ were filled with nano-TiO₂ particles, thus leading to the formation of stack holes, so the specific surface area of MZ was reduced. The schematic diagram of the nano-TiO₂ distribution in MZTC-2.5 is shown in Figure 4. It can be inferred that TiO₂ particles are homogeneously dispersed in MZTC-n (n = 0.5, 1, 2.5, 5) at the nanoscale range.

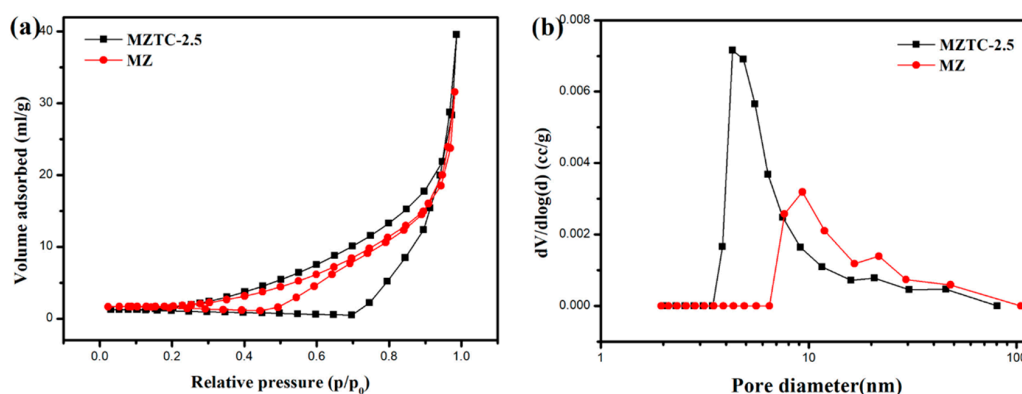


Figure 3. (a) N₂ adsorption–desorption isotherms of MZ and MZTC-2.5; (b) pore size distribution curves of MZ and MZTC-2.5.

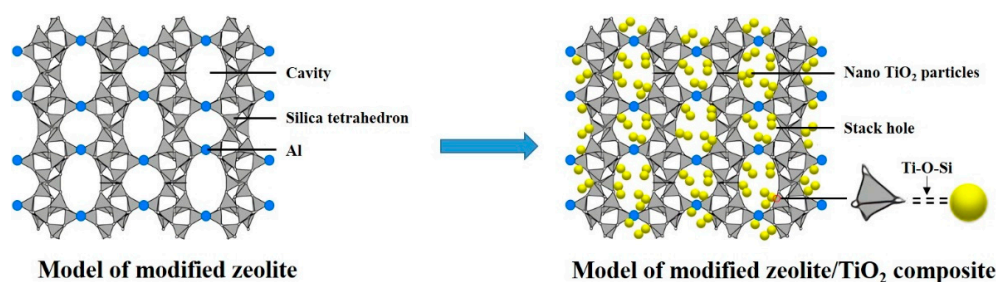


Figure 4. Models of MZ and MZTC.

Table 1. Specific surface area (S), pore volume (V) and average pore diameter (D) for MZ and MZTC-2.

Sample	S (m ² g ⁻¹)	V (cm ³ g ⁻¹)	D (nm)
MZ	392	0.29	12.02
MZTC-2.5	293	0.21	9.27

The infrared spectrum of MZTC-2.5 is shown in Figure 5. The middle infrared spectrum region (400–2000 cm⁻¹) displays the features of the chemical bonds of zeolite [45]. The absorption peaks at the range of 400–1200 cm⁻¹ are associated with the Si–O(Si) and Si–O(Al) stretching vibrations

inside the (Al,Si)O₄ tetrahedrons [46]. The infrared peaks at 1060 cm⁻¹ and 1090 cm⁻¹ are correlated with the Si–O–Si anti-symmetric stretch region of zeolite [47]. The absorption peaks at 400–600 cm⁻¹ are attributed to pseudo-lattice vibrations of structural units [48]. There is a weak absorption peak at 960 cm⁻¹ which is attributed to the anti-symmetric Ti–O–Si stretching modes of a corner-sharing tetrahedral [49,50]. It is confirmed that there is a chemical bond between TiO₂ and zeolite. TiO₂ particles are firmly fixed on the surface of zeolite with the force of a chemical bond, which is beneficial for the reclamation of photocatalysts.

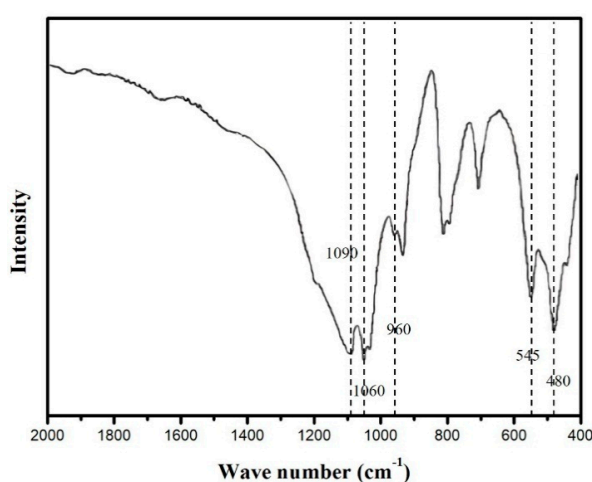


Figure 5. Infrared spectrum of MZTC-2.5.

The results of the UV–vis diffuse reflectance spectra (UV-vis DRS) of HTOP (anatase TiO₂) and MZTC-2.5 are shown in Figure 6a. It is obvious that both HTOP and MZTC-2.5 could absorb the UV-light (200–400 nm) and the absorption intensity of HTOP was almost equal to that of MZTC-2.5. The absorption peaks of HTOP and MZTC-2.5 appeared at the wavelengths of 310 nm and 345 nm, respectively. The diffuse reflectance spectra of MZTC-2.5 had a slight shift to longer wavelengths compared with that of HTOP. Similar results could be observed in other research [51,52]. It is indicated that the band-gap of MZTC-2.5 was narrowed and light with lower energy could excite the photoelectron reaction, which was probably ascribed to the existing Ti–O–Si. According to the Kubelka–Munk theory, the band-gap energies of HTOP and MZTC-2.5 could be calculated by a plot of $[A\text{h}\nu]^{1/2}$ as a function of $h\nu$, as shown in Figure 6b. The calculated band-gap energies of HTOP and MZTC-2.5 are 3.23 eV and 3.10 eV, respectively. Compared with HTOP, the band-gap of MZTC-2.5 had a slight shift towards visible light, which indicated that more light could be used to excite the photocatalysis. Hence, a better photocatalytic performance of MZTC-2.5 could be expected due to the additional state of Ti–O–Si.

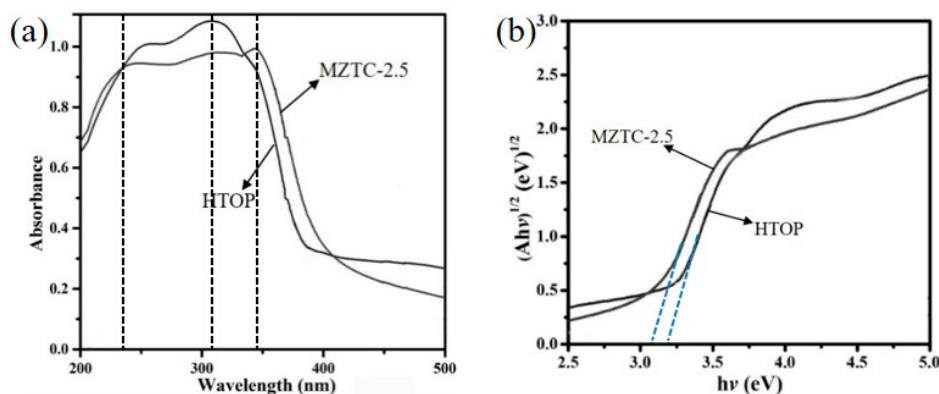


Figure 6. (a) UV–vis diffuse reflectance spectra; (b) Kubelka–Munk $(A\text{h}\nu)^{1/2}$ versus energy.

2.2. Evaluation of the Photocatalytic Efficiency

The results of the MB degradation experiment are shown in Figure 7a. In order to exclude the influence of the non-photocatalytic effects that could decrease the concentration of MB, the blank experiment was conducted. The result shows that the MB can barely be degraded by UV irradiation without a catalyst. So, the effects of photodegradation can thus be neglected in photocatalysis. The MB concentration has a slight decline with MZTC-0 added, indicating that MZ has a certain adsorption capacity, which contributes to enhance the pollutant concentration around TiO_2 [11]. Obviously, the MB degradation rate increased with the amount of loaded TiO_2 , and MZTC-2.5 showed the highest photocatalytic activity, which could remove MB up to 93.6% within 60 min. However, when the amount of loaded TiO_2 was up to 5%, the degradation rate of MZTC-5 was lower. This could be explained as the condition of low TiO_2 content, more active sites of TiO_2 would be exposed with more TiO_2 addition, while on the condition of high TiO_2 content, excess TiO_2 particles would stack and agglomerate leading to a reduction of exposed active sites. The MB degradation rate of HTOP (68%) was much lower than that of MZTC-2.5 (93.6%). This is because HTOP is prone to agglomeration in water due to the large surface energy, thus leading to a serious reduction of surface area and active sites. The MB degradation rate of NZTC-2.5 was also lower than that of MZTC-2.5, which was related with the mass transfer process. In detail, the micron-sized pores of NZTC-2.5 were obstructed due to impurities, so the transfer efficiency of MB molecules was limited. The first-order reaction kinetics model was used to fit the data obtained from the degradation experiment. The fitting curves are shown in Figure 7b, which display a good linear relationship ($R^2 > 0.98$), indicating that the photocatalytic degradation process of MB conforms to the first-order reaction kinetics. According to the fitting equation ($-\ln(C/C_0) = k \cdot t$), the slope represents the reaction rate constant k (min^{-1}). The degradation parameters are shown in Table 2. The reaction rate constant (k , 0.04694 min^{-1}) of MZTC-2.5 is 2.4 times and 1.47 times higher than that of HTOP (k , 0.01959 min^{-1}) and NZTC-2.5 (k , 0.03204 min^{-1}), respectively. The enhanced reaction rate is attributed to the synergistic effect caused by modified zeolite and nano- TiO_2 . The modified zeolite/ TiO_2 composite provides abundant TiO_2 active sites and a high concentration of pollutant, thus accelerating the photocatalysis reaction.

The results of the recycle degradation experiment of MZTC-2.5 are shown in Figure 8. The first degradation rate reached up to 93.6% for MB within 60 min. However, from the second cycle onwards, the degradation rate decreased slightly and gradually become steady. When the tests were recycled five times, the fifth degradation rate was 86.5%, which indicates the excellent recyclability of MZTC-2.5. The slight decrease in degradation rate is probably due to the occupation of TiO_2 active sites by remnant MB or the reaction products.

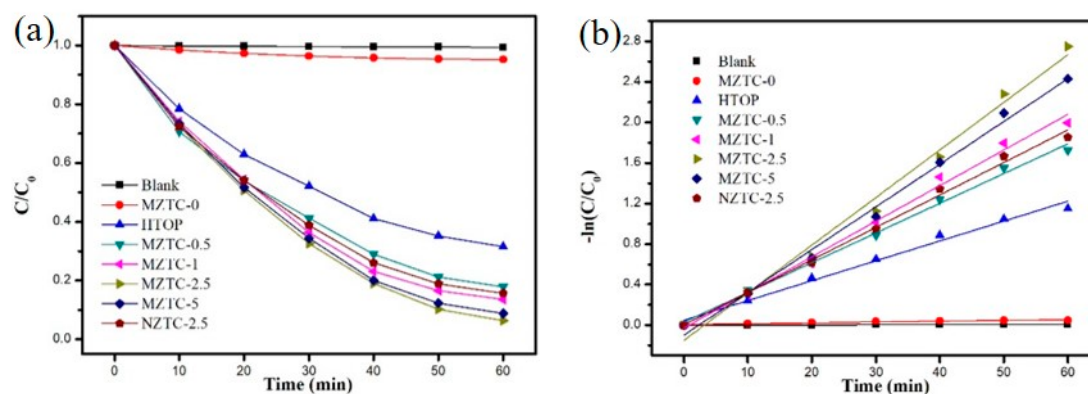


Figure 7. (a) The MB degradation rate of different samples within 60 min; (b) The corresponding linear fitting curves using the first-order reaction kinetics model.

Table 2. The parameters of the photocatalytic degradation reactions. (k = reaction rate constant; R^2 = goodness of fit).

Specimen	k (min^{-1})	R^2
Blank	9.74×10^{-4}	0.98574
MZTC-0	8.05×10^{-4}	0.98691
HTOP	0.01959	0.98693
NZTC-2.5	0.03204	0.99422
MZTC-0.5	0.02930	0.99492
MZTC-1	0.03512	0.99140
MZTC-2.5	0.04694	0.98633
MZTC-5	0.04214	0.99194

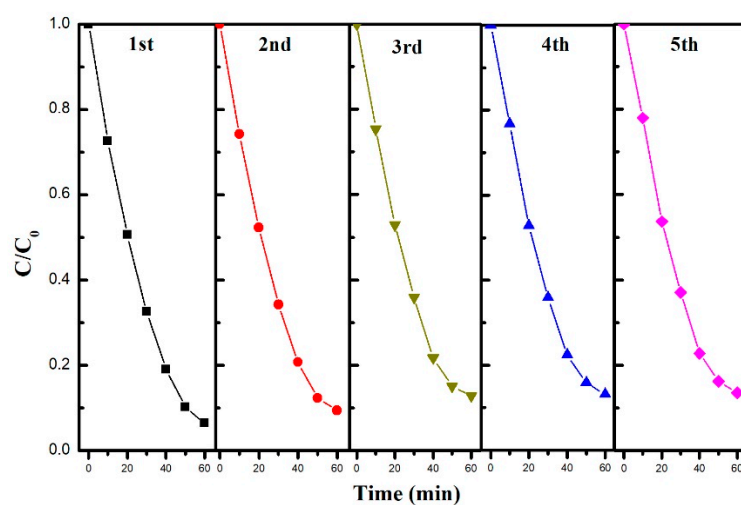


Figure 8. Results of the recycle degradation experiment of MZTC-2.5.

According to the degradation experiment results, the process of the degradation of MB can be divided into several stages in this study. Firstly, a mass of MB molecules migrate to the surface of MZTC-2.5 from the aqueous environment. Because the MB molecules have an effective molecular diameter of about 0.77 nm, which is smaller than that of MZTC-2.5 with an average pore size of approximately 9.27 nm, the MB molecules could transfer to the pores of MZTC-2.5. Due to the huge specific surface area, the adsorption equilibrium was established in a short time and MB could be stored in the large internal surfaces and on the external surfaces of MZTC-2.5, so the concentration of MB around TiO_2 was very high. Once the TiO_2 particles were illuminated by UV light, electron (e^-)–hole (h^+) pairs would be generated on the surface of TiO_2 , which would react with OH^- and the dissolved O_2 in the aqueous solution in order to generate ROS such as hydroxide radicals ($\cdot\text{OH}$), superoxide radicals (O_2^-) and hydrogen peroxide (H_2O_2) in different chain reactions. The MB would be oxidized into inorganic matter by hydroxide radicals ($\cdot\text{OH}$) as shown in Equation (1) [53,54]:



When the adsorbed MB were degraded by hydroxide radicals ($\cdot\text{OH}$), the adsorption equilibrium was broken so that more MB molecules would be captured by MZTC-2.5 and then more MB would be photocatalytically degraded. The process of degradation is shown in Figure 9.

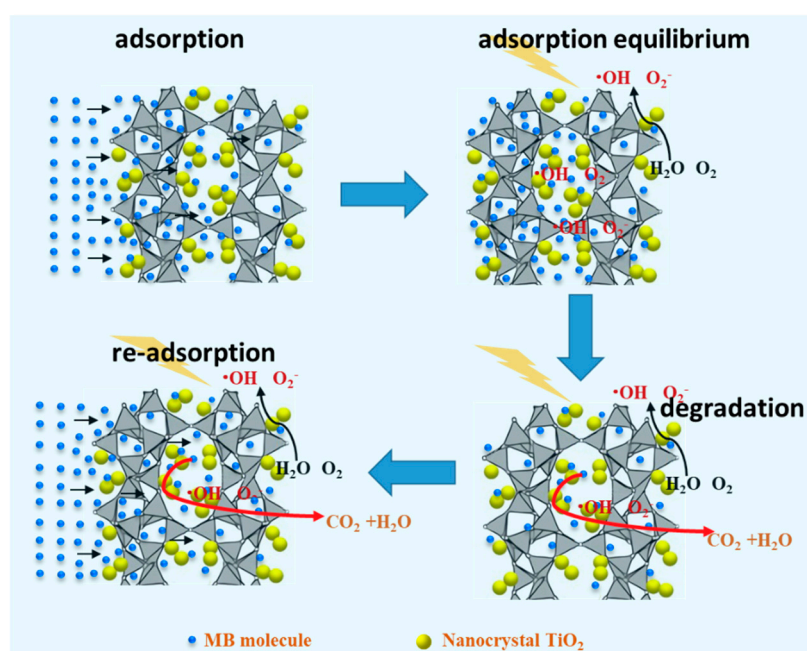


Figure 9. Mechanism of the degradation of MB in aqueous solution.

3. Experimental Procedure

3.1. Preparation of MZTC

A certain amount of NZ was immersed in the NaOH aqueous solution ($2 \text{ mol}\cdot\text{L}^{-1}$) for 6 h with continuous stirring. After alkaline erosion, the zeolite was washed using distilled water until the pH value was 7 or 8 and subsequently calcined at $400 \text{ }^\circ\text{C}$ for 2 h. The preparation of TiO_2 sol was carried out according to the literature [55]. A certain mass of Tetrabutyl Orthotitanate (TBOT) was added into distilled water dropwise with stirring. Nitric acid was also added to inhibit the hydrolysis. The weight ratio of TBOT, distilled water and nitric acid was 1:8:0.08. The white slurry was then heated in the water bath at $40 \text{ }^\circ\text{C}$ for 24 h until the sol turned light blue and transparent. Some modified zeolite (MZ) and as-prepared TiO_2 sol were mixed together with stirring and then treated with ultrasonication for 0.5 h. Afterwards, the mixture was treated in a stainless steel still under negative pressure of 0.07 MPa for 5 h. Finally, the products were dried at $105 \text{ }^\circ\text{C}$ for 2 h and then calcined at $400 \text{ }^\circ\text{C}$ for 2 h to obtain the MZTC [42]. The samples were labeled as MZTC- n ($n\%$ is the weight percentage of TiO_2 sol, i.e., $n = 0, 0.5, 1, 2.5, 5$). As a control study, the natural zeolite supported TiO_2 was also fabricated and labeled as NZTC-2.5 (NZTC=natural zeolite/ TiO_2 composite). A certain amount of the TiO_2 sol was dried at $105 \text{ }^\circ\text{C}$ for 2 h and then calcined at $400 \text{ }^\circ\text{C}$ for 2 h to obtain the TiO_2 powder, namely hydrolysis TiO_2 powder (HTOP). The chemical composition of NZ is shown in Table 3. The composition of all specimens are shown in Table 4.

Table 3. The chemical composition of natural zeolite (wt%).

SiO_2	Al_2O_3	Na_2O	CaO	K_2O	MgO	Fe_2O_3	FeO	TiO_2	P_2O_5
60–70	17.8	4.2	2.6	3.2	0.8	1.6	1.2	0.6	0.26

Table 4. Composition of the specimens. (NZTC = natural zeolite/TiO₂ composite; MZTC = modified zeolite/TiO₂ composite; HTOP = hydrolysis TiO₂ powder).

Specimen	NZ Content/wt%	MZ Content/wt%	TiO ₂ Content/wt%
HTOP	-	-	100
NZTC-2.5	93.92	-	6.08
MZTC-0	-	100	0
MZTC-0.5	-	98.72	1.28
MZTC-1	-	97.48	2.52
MZTC-2.5	-	93.92	6.08
MZTC-5	-	88.53	11.47

3.2. Characterization

The phase composition of the samples was characterized by X-ray diffraction (D/max2550, RIGAKU, Tokyo, Japan) with a Cu K α ray source (40 kV and 100 mA) at the speed of 4° min⁻¹ between 10° and 60°. The morphology of the products was observed by a scanning electron microscope (Quanta 200F, FEI, Hillsboro, OR, USA). The surface chemical composition of the samples was analyzed with an energy dispersive spectrometer (Genesis Apollo X/XL, EDAX, Berwyn, PA, USA). The specific surface area and pore size distribution of the as-prepared material were evaluated by a BET automatic nitrogen adsorption specific surface area detector (Beishide 3H-2000PS2, BEISHIDE, Beijing, China). The chemical bond between TiO₂ and zeolite was detected by Fourier transform infrared spectroscopy (EQUINOX55, BRUKER, Karlsruhe, Germany). The UV–vis diffuse reflectance spectra (DRS) were measured using a UV–VIS–NIR spectrophotometer (LAMBDA 950, PERKINELMER, Waltham, MA, USA).

3.3. Evaluation of Photocatalytic Degradation Efficiency

The photocatalytic performance of MZTC was evaluated by the MB degradation experiment. One gram of MZTC-*n* (*n* = 0, 0.5, 1, 2.5 or 5) was added into 30 mL MB aqueous solution (50 ppm), then the mixture was stirred and left in the dark for about 60 min to establish the adsorption equilibrium. Once the UV-light (125 W, 365 nm) irradiation occurred, the photocatalysis reactions started immediately. During the photocatalysis process, about 1 mL of supernatant was collected every 10 min and transferred to a quartz cuvette for the measurements of the maximum absorbance at 665 nm. According to the Lambert–Beer law, we get the relationship of $C = k'A$, so the degradation rate of MB was calculated using Equation (2):

$$\frac{C}{C_0} = \frac{A_t}{A_0} \quad (2)$$

where *C* is the concentration of MB at time *t* and *C*₀ is the concentration of initial MB. *A*_{*t*} is the absorbance of the MB aqueous solution at time *t* and *A*₀ is the absorbance of the initial MB aqueous solution. For comparison, 1 g NZTC-2.5 and 0.06 g HTOP were also tested. The mass of the HTOP used was equal to that of the TiO₂ contained in 1 g MZTC-2.5.

4. Conclusions

(1) After the modification of alkali erosion and calcination, the modified zeolite is rough and porous, which is suitable for the sedimentation of nano-TiO₂ and the diffusion of pollutants.

(2) Through the method of saturated infiltration and synthesis in situ, the modified zeolite/TiO₂ composite has been synthesized. The nano-TiO₂ are homogeneously dispersed in the structure of the modified zeolite at the nanoscale range. TiO₂ particles are firmly bonded with zeolite with the force of the chemical bond.

(3) Due to the synergistic effect comprising the uniform distribution of TiO₂ and the enhanced adsorption capacity, the MB degradation rate of MZTC-2.5 is higher than that of the equal mass of

pure TiO₂. The MB degradation rate increases with the content of TiO₂. MZTC-2.5 performs the best in terms of degradation efficiency, which could reach up to 93.6%.

(4) After five tests, the MB degradation rate of MZTC-2.5 is still 86.5%, proving that MZTC-2.5 has good recyclability.

Author Contributions: Literature search, figures, writing, G.L.; data collection, data analysis, data interpretation, W.H.; study design, Y.H.

Funding: This research was funded by Deyang science and technology plan project, grant number 11021.

Conflicts of Interest: The authors declare no conflict of interest.

References

1. Srogi, K. Monitoring of environmental exposure to polycyclic aromatic hydrocarbons: A review. *Environ. Chem. Lett.* **2007**, *5*, 169–195. [[CrossRef](#)]
2. Liu, X.; Steele, J.C.; Meng, X.Z. Usage, residue, and human health risk of antibiotics in Chinese aquaculture: A review. *Environ. Pollut.* **2017**, *223*, 161–169. [[CrossRef](#)] [[PubMed](#)]
3. Zangeneh, H.; Zinatizadeh, A.A.L.; Habibi, M.; Akia, M.; Isa, M.H. Photocatalytic oxidation of organic dyes and pollutants in wastewater using different modified titanium dioxides: A comparative review. *J. Ind. Eng. Chem.* **2015**, *26*, 1–36. [[CrossRef](#)]
4. Ahmed, S.; Rasul, M.G.; Martens, W.N.; Brown, R.; Hashib, M.A. Heterogeneous photocatalytic degradation of phenols in wastewater: A review on current status and developments. *Desalination* **2010**, *261*, 3–18. [[CrossRef](#)]
5. Huang, C.C.; Chang, H.T. Parameters for selective colorimetric sensing of mercury(II) in aqueous solutions using mercaptopropionic acid-modified gold nanoparticles. *Chem. Commun.* **2007**, *12*, 1215–1217. [[CrossRef](#)] [[PubMed](#)]
6. Noemi, R.; Moshe, A.; Gideon, O. A pilot study of constructed wetlands using duckweed (*Lemna gibba* L.) for treatment of domestic primary effluent in Israel. *Water Res.* **2004**, *38*, 2241–2248.
7. Kuriechen, S.K.; Murugesan, S. Carbon-Doped Titanium Dioxide Nanoparticles Mediated Photocatalytic Degradation of Azo Dyes Under Visible Light. *Water Air Soil Pollut.* **2013**, *224*, 1671. [[CrossRef](#)]
8. Kamegawa, T.; Kido, R.; Yamahana, D.; Yamashita, H. Design of TiO₂-zeolite composites with enhanced photocatalytic performances under irradiation of UV and visible light. *Microporous Mesoporous Mater.* **2013**, *165*, 142–147. [[CrossRef](#)]
9. Bokare, A.D.; Choi, W. Review of iron-free Fenton-like systems for activating H₂O₂ in advanced oxidation processes. *J. Hazard. Mater.* **2014**, *275*, 121–135. [[CrossRef](#)]
10. Sharma, A.; Ahmad, J.; Flora, S.J.S. Application of advanced oxidation processes and toxicity assessment of transformation products. *Environ. Res.* **2018**, *167*, 223–233. [[CrossRef](#)] [[PubMed](#)]
11. Yoneyama, H.; Torimoto, T. Titanium dioxide/adsorbent hybrid photocatalysts for photodestruction of organic substances of dilute concentrations. *Catal. Today* **2000**, *58*, 133–140. [[CrossRef](#)]
12. Karuppuchamy, S.; Iwasaki, M.; Minoura, H. Physico-chemical, photoelectrochemical and photocatalytic properties of electrodeposited nanocrystalline titanium dioxide thin films. *Vacuum* **2007**, *81*, 708–712. [[CrossRef](#)]
13. Yamaguchi, S.; Fukura, T.; Imai, Y.; Yamaura, H.; Yahiro, H. Photocatalytic activities for partial oxidation of α -methylstyrene over zeolite-supported titanium dioxide and the influence of water addition to reaction solvent. *Electrochim. Acta* **2010**, *55*, 7745–7750. [[CrossRef](#)]
14. Fuchs, V.; Méndez, L.; Blanco, M.; Pizzio, L. Mesoporous titania directly modified with tungstophosphoric acid: Synthesis, characterization and catalytic evaluation. *Appl. Catal. A Gen.* **2009**, *358*, 73–78. [[CrossRef](#)]
15. Kamegawa, T.; Sonoda, J.; Sugimura, K.; Mori, K.; Yamashita, H. Degradation of isobutanol diluted in water over visible light sensitive vanadium doped TiO₂ photocatalyst. *J. Alloys Compd.* **2009**, *486*, 685–688. [[CrossRef](#)]
16. Park, H.G.; Kim, J.I.; Kang, M.; Yeo, M.K. The effect of metal-doped TiO₂ nanoparticles on zebrafish embryogenesis. *Mol. Cell. Toxicol.* **2014**, *10*, 293–301. [[CrossRef](#)]
17. Ghosh, M.; Jana, S.C. Bi-component inorganic oxide nanofibers from gas jet fiber spinning process. *RSC Adv.* **2015**, *5*, 105313–105318. [[CrossRef](#)]

18. Gottschalk, F.; Sun, T.Y.; Nowack, B. Environmental concentrations of engineered nanomaterials: Review of modeling and analytical studies. *Environ. Pollut.* **2013**, *181*, 287–300. [[CrossRef](#)]
19. Farré, M.; Pérez, S.; Gajda-Schranz, K.; Osorio, V.; Kantiani, L.; Ginebreda, A.; Barceló, D. First determination of C60 and C70 fullerenes and N-methylfulleropyrrolidine C60 on the suspended material of wastewater effluents by liquid chromatography hybrid quadrupole linear ion trap tandem mass spectrometry. *J. Hydrol.* **2010**, *383*, 44–51. [[CrossRef](#)]
20. Domoroshchina, E.N.; Chernyshev, V.V.; Kuz'micheva, G.M.; Dorokhov, A.V.; Pirutko, L.V.; Kravchenko, G.V.; Chumakov, R.B. Changing the characteristics and properties of zeolite Y and nano-anatase in the formation of a nano-anatase/Y composite with improved photocatalytic and adsorption properties. *Appl. Nanosci.* **2018**, *8*, 19–31. [[CrossRef](#)]
21. Kuwahara, Y.; Maki, K.; Matsumura, Y.; Kamegawa, T.; Mori, K.; Yamashita, H. Hydrophobic Modification of a Mesoporous Silica Surface Using a Fluorine-Containing Silylation Agent and Its Application as an Advantageous Host Material for the TiO₂ Photocatalyst. *J. Phys. Chem. C* **2009**, *113*, 1552–1559. [[CrossRef](#)]
22. Jiang, G.; Zheng, X.; Wang, Y.; Li, T.; Sun, X. Photo-degradation of methylene blue by multi-walled carbon nanotubes/TiO₂ composites. *Powder Technol.* **2011**, *207*, 465–469. [[CrossRef](#)]
23. Torimoto, T.; Okawa, Y.; Takeda, N.; Yoneyama, H. Effect of activated carbon content in TiO₂-loaded activated carbon on photodegradation behaviors of dichloromethane. *J. Photochem. Photobiol. A Chem.* **1997**, *103*, 153–157. [[CrossRef](#)]
24. Kuwahara, Y.; Aoyama, J.; Miyakubo, K.; Eguchi, T.; Kamegawa, T.; Mori, K.; Yamashita, H. TiO₂ photocatalyst for degradation of organic compounds in water and air supported on highly hydrophobic FAU zeolite: Structural, sorptive, and photocatalytic studies. *J. Catal.* **2012**, *285*, 223–234. [[CrossRef](#)]
25. Kamegawa, T.; Yamahana, D.; Yamashita, H. Graphene Coating of TiO₂ Nanoparticles Loaded on Mesoporous Silica for Enhancement of Photocatalytic Activity. *J. Phys. Chem. C* **2010**, *114*, 15049–15053. [[CrossRef](#)]
26. Ghosh, M.; Lohrasbi, M.; Chuang, S.S.C.; Jana, S.C. Mesoporous Titanium Dioxide Nanofibers with a Significantly Enhanced Photocatalytic Activity. *ChemCatChem* **2016**, *8*, 2525–2535. [[CrossRef](#)]
27. Najafabadi, A.T.; Taghipour, F. Physicochemical impact of zeolites as the support for photocatalytic hydrogen production using solar-activated TiO₂-based nanoparticles. *ENERGY Convers. Manag.* **2014**, *82*, 106–113. [[CrossRef](#)]
28. Reddy, E.P.; Davydov, L.; Smirniotis, P. TiO₂-loaded zeolites and mesoporous materials in the sonophotocatalytic decomposition of aqueous organic pollutants: The role of the support. *Appl. Catal. B-Environ.* **2003**, *42*, 1–11. [[CrossRef](#)]
29. Al-Harbi, L.M.; Kosa, S.A.; el Maksod, I.H.A.; Hegazy, E.Z. The photocatalytic activity of TiO₂-zeolite composite for degradation of dye using synthetic UV and Jeddah sunlight. *J. Nanomater.* **2015**, *16*, 46. [[CrossRef](#)]
30. Guesh, K.; Mayoral, Á.; Márquez-Álvarez, C.; Chebude, Y.; Díaz, I. Enhanced photocatalytic activity of TiO₂ supported on zeolites tested in real wastewaters from the textile industry of Ethiopia. *Microporous Mesoporous Mater.* **2016**, *225*, 88–97. [[CrossRef](#)]
31. Li, Y.J.; Wei, C. Photocatalytic degradation of Rhodamine B using nanocrystalline TiO₂-zeolite surface composite catalysts: Effects of photocatalytic condition on degradation efficiency. *Catal. Sci. Technol.* **2011**, *1*, 802–809.
32. Liu, S.; Lim, M.; Amal, R. TiO₂-coated natural zeolite: Rapid humic acid adsorption and effective photocatalytic regeneration. *Chem. Eng. Sci.* **2014**, *105*, 46–52. [[CrossRef](#)]
33. Lafjah, M.; Djafri, F.; Bengueddach, A. Beta zeolite supported sol-gel TiO₂ materials for gas phase photocatalytic applications. *J. Hazard. Mater.* **2011**, *186*, 1218–1225. [[CrossRef](#)]
34. Domoroshchina, E.; Kravchenko, G.; Kuz'micheva, G. Nanocomposites of zeolite-titanium(IV) oxides: Preparation, characterization, adsorption, photocatalytic and bactericidal properties. *J. Cryst. Growth* **2017**, *468*, 199–203. [[CrossRef](#)]
35. Kravchenko, G.V.; Domoroshchina, E.N.; Kuz'micheva, G.M.; Gaynanova, A.A.; Amarantov, S.V.; Pirutko, L.V.; Tsybinsky, A.M.; Sadovskaya, N.V.; Kopylova, E.V. Zeolite-titanium dioxide nanocomposites: Preparation, characterization, and adsorption properties. *Nanotechnol. Russ.* **2016**, *11*, 579–592. [[CrossRef](#)]
36. Zendejdel, M.; Kalateh, Z.; Mortezaei, Z. Photocatalytic activity of the nano-sized TiO₂/NaY zeolite for removal of methylene blue. *J. Nov. Appl.* **2014**, *3*, 135–141.

37. Maraschi, F.; Sturini, M.; Speltini, A.; Pretali, L.; Profumo, A.; Pastorello, A.; Kumar, V.; Ferretti, M.; Caratto, V. TiO₂-modified zeolites for fluoroquinolones removal from wastewaters and reuse after solar light regeneration. *J. Environ. Chem. Eng.* **2014**, *2*, 2170–2176. [[CrossRef](#)]
38. Easwaramoorthi, S.; Natarajan, P. Characterisation and spectral properties of surface adsorbed phenosafranine dye in zeolite-Y and ZSM-5: Photosensitisation of embedded nanoparticles of titanium dioxide. *Microporous Mesoporous Mater.* **2009**, *117*, 541–550. [[CrossRef](#)]
39. Wang, J.-J.; Jing, Y.-H.; Ouyang, T.; Chang, C.-T. Preparation of 13X from Waste Quartz and Photocatalytic Reaction of Methyl Orange on TiO₂/ZSM-5, 13X and Y-Zeolite. *J. Nanosci. Nanotechnol.* **2015**, *15*, 6141–6149. [[CrossRef](#)]
40. Ito, M.; Fukahori, S.; Fujiwara, T. Adsorptive removal and photocatalytic decomposition of sulfamethazine in secondary effluent using TiO₂-zeolite composites. *Environ. Sci. Pollut. Res.* **2014**, *21*, 834–842. [[CrossRef](#)]
41. Jansson, I.; Suárez, S.; Garcia-Garcia, F.J.; Sánchez, B. Zeolite-TiO₂ hybrid composites for pollutant degradation in gas phase. *Appl. Catal. B Environ.* **2015**, *178*, 100–107. [[CrossRef](#)]
42. Gomez, S.; Leal, C.; Pizzio, L.; Pierella, L. Preparation and characterization of TiO₂/HZSM-11 zeolite for photodegradation of dichlorvos in aqueous solution. *J. Hazard. Mater.* **2013**, *258*, 19–26. [[CrossRef](#)] [[PubMed](#)]
43. Kruk, M.; Jaroniec, M. Gas Adsorption Characterization of Ordered Organic-Inorganic Nanocomposite Materials. *Chem. Mater.* **2001**, *13*, 3169–3183. [[CrossRef](#)]
44. Sing, K.S.; Everett, D.H.; Haul, R.A.; Moscou, L.; Pierotti, R.A.; Rouquerol, J.; Siemieniowska, T. Reporting physisorption data for gas/solid systems with Special Reference to the Determination of Surface Area and Porosity. *Pure Appl. Chem.* **1985**, *57*, 603–619. [[CrossRef](#)]
45. Mozgawa, W. The influence of some heavy metals cations on the FTIR spectra of zeolites. *J. Mol. Struct.* **2000**, *555*, 299–304. [[CrossRef](#)]
46. Pechar, F.; Rykl, D. Infrared spectra of natural zeolites of the stilbite group. *Chem. Zvesti.* **1981**, *35*, 189–202.
47. Weckhuysen, B.M.; Yu, J. Recent advances in zeolite chemistry and catalysis. *Chem. Soc. Rev.* **2015**, *44*, 7022–7024. [[CrossRef](#)] [[PubMed](#)]
48. Mozgawa, W.; Król, M.; Barczyk, K.; Science, M. FT-IR studies of zeolites from different structural groups. *Chemik* **2011**, *65*, 671–674.
49. Perego, G.; Bellussi, G.; Corno, C.; Taramasso, M.; Buonomo, F.; Esposito, A. New developments in zeolite science and technology. *Stud. Surf. Sci. Catal.* **1986**, *28*, 129–136.
50. De Man, A.J.M.; Sauer, J. Coordination, Structure, and Vibrational Spectra of Titanium in Silicates and Zeolites in Comparison with Related Molecules. An ab Initio Study. *J. Phys. Chem.* **1996**, *100*, 551–559. [[CrossRef](#)]
51. Zhang, G.; Song, A.; Duan, Y.; Zheng, S. Enhanced photocatalytic activity of TiO₂/zeolite composite for abatement of pollutants. *Microporous Mesoporous Mater.* **2017**, *255*, 61–68. [[CrossRef](#)]
52. Setthaya, N.; Chindaprasirt, P.; Yin, S.; Pimraksa, K. TiO₂-zeolite photocatalysts made of metakaolin and rice husk ash for removal of methylene blue dye. *Powder Technol.* **2017**, *313*, 417–426. [[CrossRef](#)]
53. Soltani, N.; Saion, E.; Hussein, M.Z.; Erfani, M.; Abedini, A. Visible Light-Induced Degradation of Methylene Blue in the Presence of Photocatalytic ZnS and CdS Nanoparticles. *Int. J. Mol. Sci.* **2012**, *13*, 12242–12258. [[CrossRef](#)] [[PubMed](#)]
54. Mo, J.; Zhang, Y.; Xu, Q.; Lamson, J.J.; Zhao, R. Photocatalytic purification of volatile organic compounds in indoor air: A literature review. *Atmos. Environ.* **2009**, *43*, 2229–2246. [[CrossRef](#)]
55. Yu, J.; Zhang, L.; Cheng, B.; Su, Y. Hydrothermal preparation and photocatalytic activity of hierarchically sponge-like macro-/mesoporous Titania. *J. Phys. Chem. C* **2007**, *111*, 10582–10589. [[CrossRef](#)]

